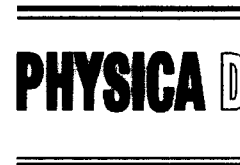




ELSEVIER

Physica D 119 (1998) 219–226



## Dynamics of one-dimensional Josephson-junction arrays

H.S.J. van der Zant<sup>a,\*</sup>, M. Barahona<sup>b,1</sup>, A.E. Duwel<sup>b</sup>, E. Trías<sup>b</sup>, T.P. Orlando<sup>b</sup>,  
Shinya Watanabe<sup>c</sup>, Steven Strogatz<sup>d</sup>

<sup>a</sup> Department of Applied Physics and DIMES, Delft University of Technology, Lorentzweg 1, 2628 CJ Delft, Netherlands

<sup>b</sup> Department of Electrical Engineering and Computer Science, MIT, Cambridge, MA 02139, USA

<sup>c</sup> Centre for Chaos and Turbulence Studies, Niels Bohr Institute, Blegdamsvej 17, Copenhagen 2100, Denmark

<sup>d</sup> Department of Theoretical and Applied Mechanics, Cornell University, Kimball Hall, Ithaca, NY 14853, USA

Received 4 August 1997; received in revised form 10 September 1997

### Abstract

We study the dynamics of one-dimensional arrays of Josephson junctions connected in parallel by superconducting wires. These arrays are model systems for the discrete, damped sine-Gordon equation and excellent agreement between theory and experiment is obtained. The influence of boundary conditions and the coupling between two discrete sine-Gordon systems have also been investigated. In Josephson ladders, superconducting islands are connected to other islands by three Josephson junctions. The dynamics of Josephson ladders is more complicated than that of the purely 1D sine-Gordon systems. © 1998 Elsevier Science B.V.

### 1. Introduction

Long Josephson junctions have long been a model system for the continuous sine-Gordon equation. Their discrete counterparts, one-dimensional (1D) arrays of Josephson junctions were less studied because they were much harder to fabricate in a uniform way. Nowadays, a niobium technology to fabricate discrete arrays is available even commercially. Single flux quantum logic is based on discrete arrays of overdamped Josephson junctions and requires a very small window for junction parameters. The spread in junction parameters has been reduced to 5–10% and

arrays can be made in any desired planar geometry.

An essential feature introduced by discreteness is the generation of radiation by a moving kink. Early simulations by Currie et al. [1] showed that when a kink propagates in a highly discrete one-dimensional lattice, it excites small-amplitude linear waves in its wake. This effect was explained analytically by Peyrard and Kruskal [2], who also found that in the absence of external driving, kinks propagate preferentially at a particular set of velocities. In discrete systems the dispersion relation for these small amplitude waves is sinusoidal. It is this sinusoidal relation that allows for the coupling to moving kinks, thus leading to new resonances and dynamics.

Various Josephson-junction arrays are depicted in Fig. 1. Different geometries induce different boundary conditions (Figs. 1(a) and (b)), or two discrete sine-Gordon equations (DSGEs) may be coupled (Fig. 1(d))

\* Corresponding author. Tel.: +31 15 278 6075; fax: +31 15 278 3251; e-mail: herre.@qt.tn.tudelft.nl.

<sup>1</sup> Present address: Ginzton Laboratory, Stanford University, Stanford, CA 94305, USA.

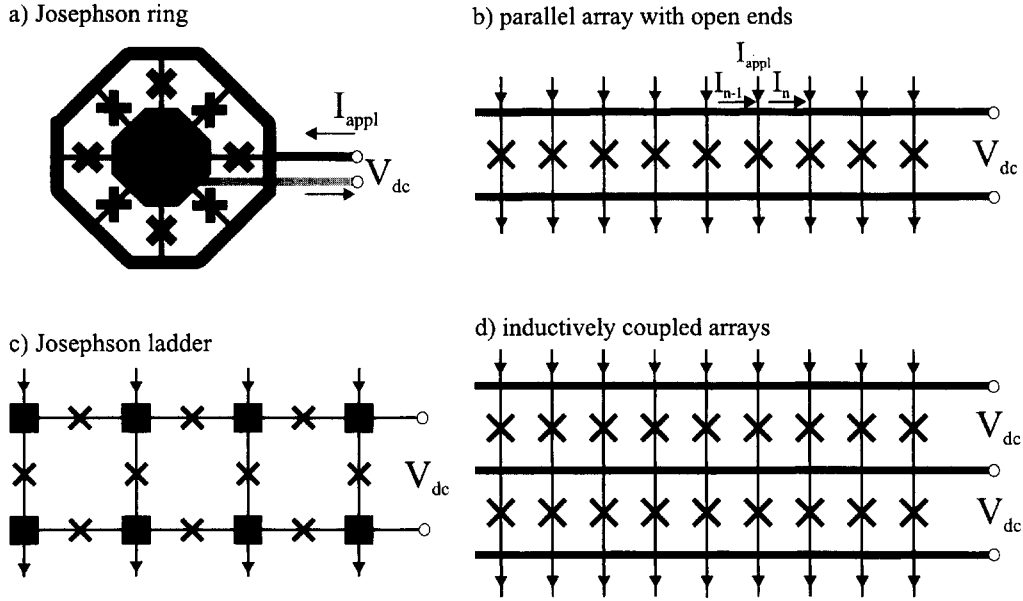


Fig. 1. Various one-dimensional Josephson-junction arrays. Crosses represent the Josephson junctions.

or a nonlinear term may arise due to the presence of junctions in the horizontal branches (Fig. 1(c)). In this paper we will discuss the measured properties of these 1D Josephson arrays which are moderately underdamped. Before discussing the measurements, we first introduce the DSGE and explain some of the experimental aspects.

## 2. Josephson arrays as model systems for the DSGE

The governing equations which model Josephson arrays are derived by applying Kirchhoff's current law (see Fig. 1(b)),  $I_{n-1} + I_{\text{appl}} = I_n + I_{\text{junction}}$ , the RCSJ model for the current through a single junction

$$I_{\text{junction}} = C\dot{V}_n + V_n/R + I_c \sin \phi_n, \quad (1)$$

the Josephson equation,  $V_n = \Phi_0 \dot{\phi}_n / 2\pi$ , and fluxoid quantization:

$$\sum_{\text{loop}} \phi_n = 2\pi \frac{\Phi_{\text{loop}}}{\Phi_0} = \frac{2\pi}{\Phi_0} [\Phi_{\text{appl}} + \Phi_n^{\text{self}}]. \quad (2)$$

Here,  $I_{\text{appl}}$  is the applied current per node,  $\phi_n$  the gauge invariant phase difference,  $V_n$  the voltage across junction  $n$ ,  $C$  the junction capacitance,  $R$  its resistance and  $I_c$  is the junction critical current. The perpendicular applied magnetic field  $\Phi_{\text{appl}}$  is generally expressed as the quantity  $f$ , the applied flux per cell normalized to the flux quantum  $\Phi_0 = h/2e$ . The magnetic fields induced by the currents in the array (self-fields) can be written as

$$\Phi_n^{\text{self}} = L_s I_n^{\text{loop}} + \sum_{n \neq m} L_{m,n} I_m^{\text{loop}}, \quad (3)$$

where  $L_s$  is the self-inductance of a cell and  $L_{m,n}$  is the mutual inductance between cell  $m$  and  $n$ . Our numerical code can include longer range inductances as necessary, up to the full inductance matrix. For 1D systems, however, we found that just including self-inductances already reproduces the measurements accurately.

We first apply these equations to a one-dimensional array of  $N$  Josephson junctions connected in parallel by superconducting wires as illustrated in Figs. 1(a) and (b). The superconducting wires can be viewed as inductors. When taking only the self-inductance

into account, the damped, driven, discrete sine-Gordon model is obtained:

$$\ddot{\phi}_n + \Gamma \dot{\phi}_n + \sin \phi_n = I_{\text{appl}}/I_c + \Lambda_J^2 (\phi_{n+1} - 2\phi_n + \phi_{n-1}) \quad (4)$$

for  $j = 1, \dots, N$ .  $\Gamma$  characterizes the damping in the system and  $\Lambda_J$  is a measure of the discreteness. The smaller the  $\Lambda_J$ , the more discrete the system is. We have normalized the current to  $I_c$ , the voltage to  $I_c R_n$ , and time ( $t$ ) to  $1/\omega_p = \sqrt{L_J C}$  (inverse plasma frequency). Here,  $R_n$  is the normal-state junction resistance and  $L_J$  is the Josephson inductance,  $L_J = \Phi_0/(2\pi I_c)$ . The boundary conditions for Eq. (4) will be discussed in later sections.

Our samples were fabricated using a niobium tri-layer process [3]. The junctions are  $3 \times 3 \mu\text{m}^2$  and cell sizes ( $p$ ) are of the order of  $10 \mu\text{m}$ . Junction parameters have been determined using the diagnostic procedures described elsewhere [4]. Typical numbers for our arrays are  $R \approx 100 \Omega$ ,  $C \approx 300 \text{ fF}$ ,  $I_c \approx 10 \mu\text{A}$ , and  $L_s \approx 10 \text{ pH}$ . With these numbers  $\Gamma = (\Phi_0/(2\pi I_c R^2 C))^{1/2} \approx 0.1$  and  $\Lambda_J^2 = L_J/L_s \approx 3$  so that our arrays are underdamped and moderately discrete.

In the experiment, one usually measures the dc voltage across the array ( $V_{\text{dc}}$ ) as a function of the applied current through the array. The ac components are much harder to measure since  $\omega_p$  is typically 300 GHz. The number of kinks in the system can be controlled by the perpendicular magnetic field. The damping  $\Gamma$  and discreteness parameter  $\Lambda_J$  can be changed by varying the critical current density (a fabrication process parameter that is varied in the range 100–5000 A/cm<sup>2</sup>). The critical current is temperature dependent which allows us to change  $\Gamma$  and  $\Lambda_J$  simultaneously by varying the temperature.

### 3. Dynamics of Josephson rings: DSGE with periodic boundary conditions

The ring geometry introduces a topological constraint:

$$\phi_{n+N} = \phi_n + 2\pi M, \quad (5)$$

where  $M$  is the number of kinks or vortices trapped in the ring. Without loss of generality,  $M$  can be restricted to  $M = 0, \dots, [N/2]$  due to the symmetry of Eqs. (4) and (5).  $M$  is determined by the initial conditions, but it remains constant as the system evolves.

Fig. 2(a) plots  $I$ – $V$  curves of a Josephson ring cooled down in different magnetic fields applied perpendicular to the ring and junctions. Cooling down in a field of *about*  $M$  flux quanta  $\Phi_0$  corresponds to trapping *exactly*  $M$  vortices in the ring. When the ring is cooled through the critical temperature of niobium ( $T_c$ ) in zero field, the  $I$ – $V$  curve shows a critical current and jumps to the gap voltage at  $0.84NI_c$ . When cooling through  $T_c$  with  $M = 1$  applied to the ring, the critical current vanishes and a current step appears near  $V = 0.2 \text{ mV}$ . The jump to the gap voltage now occurs at  $I_{\text{max}} = 0.55NI_c$ . With  $M = 2, 3$  and  $4$  applied to the ring, the voltage position of the steps increases to 0.35, 0.43 and 0.48 mV, respectively. The  $I$ – $V$  for  $5\Phi_0$  is identical to the one when cooling down with  $3\Phi_0$ .

In contrast to experiments on continuous Josephson rings [5,6], the voltages of the steps shown in Fig. 2(a) are not linear in  $M$ . We have performed [7] a linear analysis ( $\Lambda_J^2 \gg 1$ ) of 1D parallel arrays with free boundaries. In such a system, resonances occur at voltages determined by the dispersion relation  $\omega(k)$  of a 1D discrete, linear transmission line of inductances  $L_s$  and capacitances  $C$ . A similar analysis for a ring yields that the resonant voltage peaks  $V_M$  are given by

$$\frac{V_M}{V_0} = 2 |\sin(M\pi/N)|, \quad (6)$$

where  $V_0 = \Phi_0\omega_0/2\pi$  with  $\omega_0 = \sqrt{L_s C}$ . In the inset of Fig. 2(a), we plot the voltage position of the resonances as a function of  $M$ . The solid line in this inset is Eq. (6) with a fitting parameter  $V_0 = 0.25 \text{ mV}$ . Near the Brillouin zone edges ( $M = 3, 4$ ), small deviations from the sinusoidal dependence are found. Including mutual-inductance interactions between cells in the ring explains this effect quantitatively.

In Fig. 2(a), one clearly sees that the  $M = 1$  step contains smaller steps. These steps are enlarged in Fig. 2(b). For high  $\Lambda_J^2$  (high temperatures; not shown in the figure) the  $I$ – $V$  curve is smooth indicating a

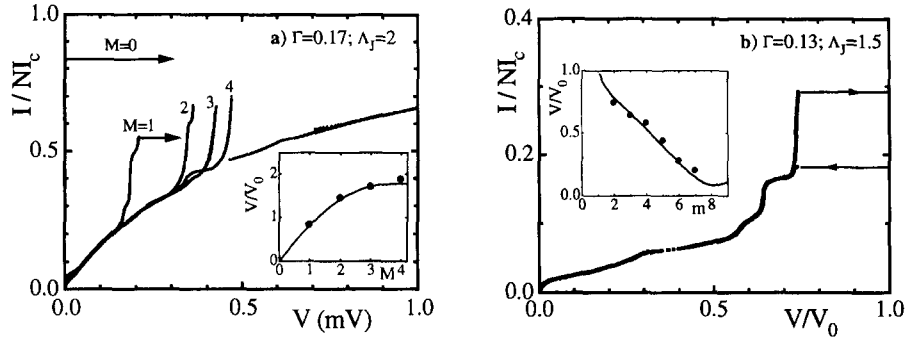


Fig. 2. (a) Experimental  $I$ - $V$  curves corresponding to the five possible situations with  $M$  kinks trapped in a ring of  $N = 8$  junctions. Inset: voltage position of main steps versus  $M$ . Curve is Eq. (6) with  $V_0 = 0.25$  mV. (b) Enlarged view of the curve with  $M = 1$  taken at a slightly lower temperature. Inset: voltage position of the substructure versus  $m$ . Curve is Eq. (7) with  $V_0 = 0.25$  mV.

continuous acceleration of the vortex. However, as  $\Lambda_J^2$  approaches 1, substructure becomes visible in the  $I$ - $V$  characteristic and in Fig. 2(b) six resonant steps are present. The substructure is caused by a phase locking between the propagating kink and the linear waves it excites in its wake [8]: damping is low in our systems and consequently, the oscillations the kink generated have not died out before the kink passes by again. The possible ringing frequencies are the lattice eigenfrequencies of small oscillations about the kink, and the circulation frequency of the kink is proportional to the voltage position of the step. By matching the circulation period to an integer multiple  $m$  of ringing periods, the following formula is obtained for the resonant voltages [9]:

$$\frac{V_m}{V_0} = \frac{1}{m} [\Lambda_J^{-2} + 4 \sin^2(\pi m/N)]^{1/2}. \quad (7)$$

In the inset of Fig. 2(b), the drawn line is Eq. (7) with  $V_0 = 0.25$  mV. There is a good agreement between the model and our experiment.

Our simulations [8,10] indicate that in the region for “low” voltages ( $V < V_M$ ) kinks in discrete systems maintain their characteristic kink-like shape but with small-amplitude oscillations superimposed on their wave form. The linear waves are phase-locked to the kink and together they form a traveling wave. We found that for “high” voltages ( $V > V_M$ ) the behavior is qualitatively different: now the vortex stretches over the whole system, that is  $\phi_n(t) \approx$

$2\pi V_{dc}t/\Phi_0 + kpn$ , where  $k$  is the wave number. We will call this the whirling state. Here, the periodic motion of a vortex can be destabilized by parametric resonance, leading to quasiperiodic and highly irregular behavior [10,11].

Fig. 3(a) shows the  $I$ - $V$  curve of a Josephson ring with  $M = 0$ . Starting from  $I = 0$ , the array remains in the superconducting state up to  $I = 37 \mu\text{A}$ . In the superconducting state the system has a stable static solution with all the junctions in phase:  $\phi_n = \sin^{-1} I/I_c$  for all  $n$ . At  $I = 37 \mu\text{A}$  the jump to the steep gap region occurs and the junction phase changes continuously in time (whirling state). The upgoing part of the  $I$ - $V$  is smooth, but when  $I$  is decreased, there are current steps at 0.93, 0.71 and 0.35 mV. As shown in Fig. 3(a), there is hysteresis when biasing on these smaller steps.

To understand the origin of these steps, we have performed a stability analysis of the in-phase whirling solution  $\phi^*(t)$ . Let  $\phi_n(t) = \phi^*(t) + u_n(t)$ , where  $u_n(t)$  is a small perturbation. Then

$$\begin{aligned} \ddot{u}_n + \Gamma \dot{u}_n + [\cos \phi^*(t)] u_n \\ = \Lambda_J^2 [u_{n+1} - 2u_n + u_{n-1}]. \end{aligned} \quad (8)$$

The boundary conditions are periodic:  $u_{n+N} = u_n$ . As long as  $I$  is not too small, the whirling solution may be approximated by  $\phi^*(t) \approx \omega t$ , where  $\omega = 2\pi/T$  with  $T$  the oscillation period. Expand  $u_n(t)$  as a discrete Fourier series in space:  $u_n(t) =$

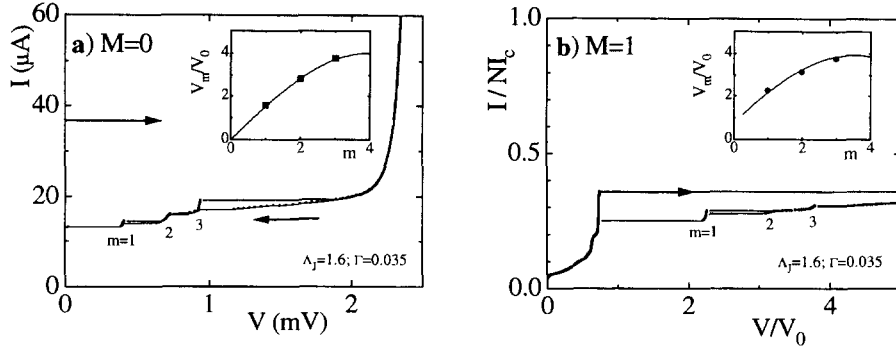


Fig. 3. (a) Experimental  $M = 0$   $I$ - $V$  curve of the same Josephson ring as in Fig. 2 showing three resonant steps in the high-voltage region. Inset: dots are measured voltage positions of the steps versus mode number  $m$ ; curve is leading order estimate  $\omega = 2\omega_m$ . (b)  $I$ - $V$  curve of the same sample for  $M = 1$  again showing three resonant steps in the high-voltage region. Inset: dots are measured voltage positions of the steps versus mode number  $m$ ; curve is leading order estimate  $\omega = \omega_m + \omega_{m+M}$ .

$\sum_{m=0}^{N-1} A_m(t) \exp(2\pi imn/N)$ . Then the modes decouple:

$$\ddot{A}_m + \Gamma \dot{A}_m + [\omega_m^2 + \cos \omega t] A_m = 0 \quad (9)$$

for  $m = 0, \dots, N-1$ , where  $\omega_m = 2\omega_0 |\sin(m\pi/N)|$  is the lattice eigenfrequency of mode  $m$ .

Eq. (9) is a damped Mathieu equation. For certain values of the parameters,  $A_m(t)$  grows exponentially in which case the in-phase whirling solution is *unstable* to the growth of mode  $m$ . These parametric instabilities occur only at certain rotation frequencies  $\omega$  that resonate with the lattice eigenfrequencies, namely (for  $\Lambda_J^2 > 1$ ):

$$\omega \approx 2\omega_m = 4\omega_0 |\sin(m\pi/N)|. \quad (10)$$

This resonance occurs for each  $m = 0, \dots, N-1$ , but at most  $[N/2] + 1$  of these can be observed since  $\omega_{N-m} = \omega_m$ . The inset of Fig. 3(a) shows the voltage position of the steps as a function of the mode number  $m$ . The voltage is normalized to the measured  $V_0$  of 0.25 mV. The solid line in the inset is the predicted resonance frequency  $\omega = 2\omega_m$ ; no fitting parameters were used. We find a close agreement between the data and our model.

Similar steps are also observed for  $M > 0$ . An example is shown in Fig. 3(b) for the same ring with  $M = 1$ . For low voltages, a current step occurs at  $V = 0.75V_0$  which is due to the propagation of a single vortex. The whirling state is found for  $V > 0.75V_0$  and

in the return path of this state, three resonant steps are visible. We have generalized our linear stability analysis to the case  $M > 0$ . Instabilities are expected [11] to occur at  $\omega \approx [\omega_m + \omega_{m+M}]$ . The inset of Fig. 3(b) shows that the locations of the steps in the experiment (solid circles) are well explained by our theory (solid line).

#### 4. Open-ended Josephson arrays: DSGE with open boundaries

With only self-inductance, the boundary conditions of open-ended Josephson arrays are

$$\begin{aligned} \phi_0(t) &= \phi_1(t) - 2\pi f, \\ \phi_{N+1}(t) &= \phi_N(t) + 2\pi f \end{aligned} \quad (11)$$

for all  $t$ , where artificial junctions  $\phi_0$  and  $\phi_{N+1}$  are introduced at the endpoints so that (4) is valid at  $n = 1$  and  $N$  as well [10]. In contrast to Josephson rings,  $f$  can vary *continuously* and, by symmetry, it can be restricted to  $0 \leq f \leq 1/2$ .

In zero field, the  $I$ - $V$  characteristic displays the same characteristic features as the  $M = 0$  curve for the rings. After reaching a large critical current, the system switches to the whirling branch and steps are visible in the return path. In open-ended systems, the wave vectors are however different and steps are expected at voltages  $V_m = \Phi_0 \omega_m / 2\pi$  with

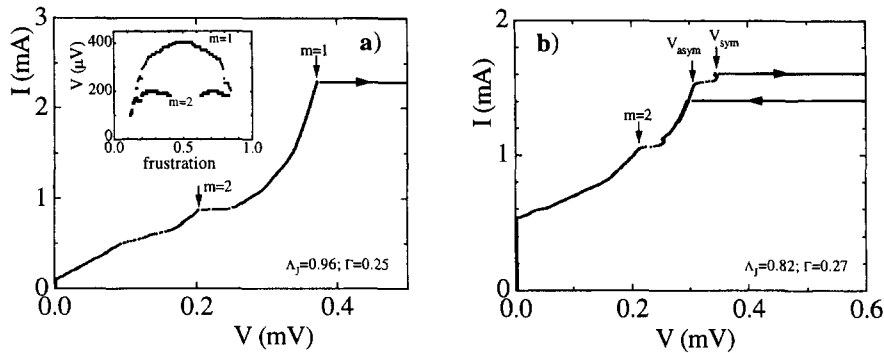


Fig. 4. (a) Experimental  $I$ - $V$  curve of a 1D parallel array with 54 Josephson junctions showing the main Eck step at  $V = 0.38$  mV and sub steps below this voltage. Inset: Measured voltages of the Eck peak ( $m = 1$  step) and the  $m = 2$  step versus frustration. (b) Experimental  $I$ - $V$  curve of an inductively coupled Josephson array ( $2 \times 54$ ) measured across one of the rows.

$\omega_m = 2\omega_0 |\sin(m\pi/2N)|$ . In total  $N - 1$  steps are expected. We have observed 8 steps in an open-ended array with  $N = 9$  and found very good agreement between the data and the theory [10]. Note that, these steps also exist in long continuous Josephson junctions (zero-field steps) showing that the parametric destabilization discussed in Section 3 is not an effect caused by discreteness.

In a perpendicular magnetic field vortices (kinks) are introduced in the system above a critical value corresponding to  $f_{c1} \approx 2/(\pi^2 \Lambda_J)$ .<sup>2</sup> We can now distinguish two different regimes. In short systems, Fiske modes are generally observed [7]. Fiske resonances can be described as cavity-mode resonances resulting from boundary reflections when kinks pass through the array. The wavelength of the excited modes is therefore given by  $\lambda = 2N/m$  so that the resonance voltage locations do not depend on  $f$ :

$$\frac{V_{\text{Fiske}}}{V_0} = 2 |\sin(m\pi/2N)|. \quad (12)$$

As  $N$  becomes large, these Fiske resonances disappear due to damping of the edge reflections. Now, only a single resonant peak is observed in the  $I$ - $V$  characteristic whose position shifts with magnetic field. The

<sup>2</sup>  $f_{c1}$  is calculated using the analogy with single long Josephson junctions. For a long Josephson-junction the entry field is equal to  $B_{c1} = 2\Phi_0/\pi^2 \lambda_J h_{\text{eff}}$ , where  $h_{\text{eff}}$  is the effective barrier thickness (see for example [12, Eq. (8.157)]). Going from the continuous case to the discrete case one should replace  $\lambda_J$  by  $\Lambda_J$  and  $h_{\text{eff}}$  by  $p$ .

position of this Eck-peak can be calculated by noting that in a magnetic field an array of kinks almost forms a sinusoidal wave with wave number  $kp = 2\pi f$ . A linear analysis then yields the position of the Eck voltage [13]:

$$\frac{V_{\text{Eck}}}{V_0} = 2 |\sin(\pi f)|. \quad (13)$$

In Fig. 4(a), we plot a typical  $I$ - $V$  for a long discrete Josephson array with  $N = 54$ . One clearly observes the main resonant peak near  $V = 0.38$  mV. In the inset, the voltage position of this step is plotted as a function of  $f$ . As expected, the Eck peak voltage is periodic in  $f$  with period  $f = 1$  and is approximately symmetric with respect to  $f = 0.5$ . On the main step, substructure is visible at lower voltages. These steps are not Fiske steps since their position changes with magnetic field as shown in the inset of Fig. 4(a). The second step achieves the maximum voltage near  $f = 0.25$ , and it disappears near  $f = 0.5$  and for approximately  $f < f_{c1}$ .

Our numerical simulations [14] show that on these sub steps the solutions look like trains of kinks (traveling wave with  $x/p = \omega t + 2\pi fn$ ), phase-locked by a finite amplitude radiation. The situation is very similar to that of a Josephson ring: in the ring a kink interacts with the oscillatory wave it leaves behind. In the open-ended system, an array of kinks periodically kicks a junction and the oscillatory wave it creates behind is felt by the next kink that comes by. The

Eck ( $m = 1$ ) steps are ubiquitous in one-dimensional parallel arrays as well as in continuous long junctions. In contrast, the  $m > 1$  steps do not appear in long continuous junctions.

### 5. Inductively coupled arrays: Coupled DSGEs

When two one-dimensional arrays are brought closer together, their magnetic fields may couple. The interactions will be the strongest when the two arrays share the middle superconducting wire as illustrated in Fig. 1(d). Currents through this wire will induce self-magnetic fields in both arrays (inter-row coupling). With a mutual inductance of  $M_v$  between adjacent cells in the vertical direction, inductively coupled arrays are described by two coupled driven and damped DSGEs. Defining  $\eta(\phi) = \ddot{\phi}_n + \Gamma \dot{\phi}_n + I_c \sin(\phi_n)$  and  $\nabla^2 \phi = \phi_{n+1} - 2\phi_n + \phi_{n-1}$ , one obtains:

$$\eta(\phi) + M_v \eta(\psi) = \Lambda_J^2 \nabla^2 \phi + I_{\text{appl}}/I_c, \quad (14)$$

$$\eta(\psi) + M_v \eta(\phi) = \Lambda_J^2 \nabla^2 \psi + I_{\text{appl}}/I_c. \quad (15)$$

The essential feature introduced by the coupling is that it controls the phase between solutions of each row. A linear analysis yields two possible phase relations. In the antisymmetric mode the phase oscillations of two junctions in the vertical direction, are shifted by  $\pi$ . In the symmetric mode, the phase oscillations are in-phase. One can also visualize the in-phase solution as two arrays of kinks, one in each Josephson line, which are situated exactly on top of each other. In the antisymmetric mode, they are shifted with respect to each other. In an experiment, the two different modes can clearly be observed. In the antisymmetric mode, the kinks reach a lower limiting velocity than in the symmetric mode. The larger the  $M_v$ , the larger the difference in limiting velocities. As a consequence, the Eck peak is split into two separate peaks as illustrated in Fig. 4(b). The positions of the resonances can be calculated straightforwardly [15,16] and agree well with our data.

Like in the single long arrays, higher harmonics  $m > 1$  steps are observed as  $\Lambda_J$  is reduced below 1. The  $m = 2$  step may be important for high-frequency oscillator applications of these arrays. To obtain small

linewidths and high output power levels, one would like to have many arrays phase-locked to each other. The symmetric mode is the most promising in this respect but in actual arrays this in-phase mode is difficult to stabilize. Numerical simulations show that the  $m = 2$  mode contains two harmonics with large-amplitude oscillations. For the higher harmonic the rows are phase-locked and are in-phase. The  $m = 2$  step is very stable in the experiment. There is no splitting of the  $m = 2$  step. Such a splitting is expected from theory and at this moment, it is unclear why this splitting does not occur.

### 6. Beyond one-dimensional arrays: Josephson ladders

Josephson ladders are one-dimensional arrays with junctions added in the horizontal branches. If the junction area of the horizontal junction is smaller than for the vertical junctions, the coupling in the horizontal direction is effectively reduced. With a weaker coupling in the horizontal direction, the static properties of anisotropic ladder networks can be described by a discrete sine Gordon equation with the discreteness parameter replaced by the ratio of the coupling in the horizontal and the vertical directions [17]. When considering dynamical properties of Josephson ladders, an approach based on the DSGE is clearly an oversimplification. The phase differences across horizontal junctions can be substantial. It turns out that the dynamics of Josephson ladders is more complex than that of 1D parallel arrays [18,19].

In a magnetic field of  $f = 1/2$ , one of the solutions for the isotropic Josephson ladder can be reduced to a system of three coupled nonlinear pendulum equations [18]:

$$\ddot{\phi} + \Gamma \dot{\phi} - \sin \theta \sin \phi = I_{\text{appl}}, \quad (16)$$

$$\ddot{\theta} + \Gamma \dot{\theta} + \cos \phi \cos \theta = -4\Lambda_J^2 (\theta + \varphi), \quad (17)$$

$$\ddot{\varphi} + \Gamma \dot{\varphi} + \sin \varphi = -2\Lambda_J^2 (\theta + \varphi), \quad (18)$$

where  $\phi$  is the average of the vertical phases in a cell  $(\phi_1 + \phi_2)/2$ ,  $\theta = (\phi_1 - \phi_2 - \pi)/2$  and  $\varphi$  is the phase of the top row (for  $f = 1/2$ , the bottom row has a phase difference of  $-\varphi$ ). Our simulations show that we can regard both  $\varphi$  and  $\theta$  as small

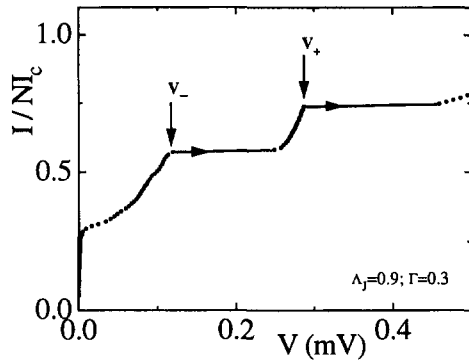


Fig. 5. Experimental  $I$ - $V$  curve of a Josephson ladder of seven cells taken at  $f = 1/2$ .

oscillations driven by the whirling mode  $\phi$ . Then, the last two equations can be linearized and in the limit for small damping, these two equations have two resonant frequencies:  $V_- \approx \sqrt{2/3} \Phi_0 / (2\pi \sqrt{L_J(T)C})$  and  $V_+ \approx \sqrt{6} \Phi_0 / (2\pi \sqrt{L_s C})$ . In Fig. 5, we plot an  $I$ - $V$  characteristic of a Josephson ladder in a magnetic field of  $f = 1/2$ . One clearly observes the two resonant peaks  $V_-$  and  $V_+$ . As expected,  $V_-$  shifts with temperature because the Josephson inductance  $L_J$  is temperature-dependent. In contrast,  $V_+$  is almost temperature-independent. The peak positions in the experiment agree well with our predictions.

Eqs. (16)–(18) are more general, and when geometrical factors are included, they can be used to describe various Josephson arrays at  $f = 1/2$ . For example, 1D parallel arrays are given by Eqs. (16) and (17) disregarding the  $\varphi$  on the right-hand side. The main resonance is the Eck peak ( $V_+$ ) and there is no equivalent step that corresponds to  $V_-$ . In the limit where inductances can be neglected, Eqs. (17) and (18) can be combined and there is only one single resonant frequency giving rise to the  $V_-$  step. The moving kinks now excite ringing oscillations of the junctions at an eigenfrequency close to  $\omega_p$ . In Josephson ladders with self-inductance, both horizontal junctions and the inductances play a role and therefore both  $V_-$  and  $V_+$  are observed. Two-dimensional Josephson arrays act in this respect similarly to Josephson ladders: both  $V_-$  and  $V_+$  can be observed.

These observations clearly show that Josephson ladders are interesting model systems intermediate

between the purely 1D discrete sine-Gordon systems and 2D arrays. The dynamics is complicated but the example above shows that analytical results are possible in some cases. On the other hand, the ladders themselves may prove to be interesting systems for nonlinear dynamic studies. For example, when ac currents are applied to anisotropic ladders, Floría et al. [19] have discussed the existence of intrinsic localized modes (discrete breathers). The experimental verification of such localized modes should in principle be possible but we require a better understanding of the dynamics of ac driven Josephson ladders.

### Acknowledgements

We acknowledge the support of the NSF Graduate Fellowship program and NSF Grants DMR-9402020, DMR-9610042, DMS-9057433, and DMS-9500948 and the Dutch Foundation for Fundamental Research on Matter (FOM).

### References

- [1] J.F. Currie, S.E. Trullinger, A.R. Bishop, J.A. Krumhansl, *Phys. Rev. B* 15 (1977) 5567.
- [2] M. Peyrard, M.D. Kruskal, *Physica D* 14 (1984) 88.
- [3] HYPRES, Inc., Elmsford, NY 10523.
- [4] H.S.J. van der Zant et al., *Appl. Phys. Lett.* 65 (1994) 2102.
- [5] A. Davidson, B. Dueholm, N.F. Pedersen, *J. Appl. Phys.* 60 (1986) 1447.
- [6] A.V. Ustinov et al., *Phys. Rev. Lett.* 69 (1992) 1815.
- [7] H.S.J. van der Zant et al., *Phys. Rev. B* 49 (1994) 12945.
- [8] H.S.J. van der Zant et al., *Phys. Rev. Lett.* 74 (1995) 174.
- [9] A.V. Ustinov, M. Cirillo, B.A. Malomed, *Phys. Rev. B* 47 (1993) 8357.
- [10] S. Watanabe et al., *Physica D* 97 (1996) 429.
- [11] S. Watanabe et al., *Phys. Rev. Lett.* 74 (1995) 379.
- [12] T.P. Orlando, K.A. Delin, *Foundations of Applied Superconductivity*, Addison-Wesley, Reading, MA, 1991.
- [13] H.S.J. van der Zant, T.P. Orlando, *J. Appl. Phys.* 76 (1994) 7605.
- [14] A.E. Duwel et al., *J. Appl. Phys.* 82 (1997) 4661.
- [15] A.E. Duwel et al., *J. Appl. Phys.* 79 (1996) 7864.
- [16] A. Petraglia et al., *Phys. Rev. B* 55 (1997) 8490.
- [17] M. Kardar, *Phys. Rev. B* 33 (1986) 3125; J.J. Mazo, F. Faló, L.M. Floría, *Phys. Rev. B* 52 (1995) 10433; C. Denniston, C. Tang, *Phys. Rev. Lett.* 75 (1995) 3930.
- [18] M. Barahona et al., *Phys. Rev. B* 55 (1997) R11989.
- [19] L.M. Floría et al., *Europhys. Lett.* 36 (1996) 539; P.J. Martínez et al., *Physica D* 119 (1998) 175.